Revealing antiphase-domain dynamics in alloys by combining advanced statistical techniques with x-ray photon correlation spectroscopy

Lorenz-M. Stadler,[1,*] Bogdan Sepiol,[1] Jan W. Kantelhardt,[2] Ivo Zizak,[3] Gerhard Grübel,[4,†] and Gero Vogl[1]
[1]*Institut für Materialphysik, Universität Wien, Strudlhofgasse 4, A-1090 Wien, Austria*
[2]*Fachgruppe Theorie, Fachbereich Physik und Zentrum für Computational Nanoscience, Martin-Luther-Universität Halle-Wittenberg, D-06099 Halle, Germany*
[3]*Hahn-Meitner-Institut Berlin, Glienicker Straße 100, D-14109 Berlin, Germany*
[4]*European Synchrotron Radiation Facility, BP 220, F-38043 Grenoble Cedex, France*
(Received 23 January 2004; published 16 June 2004)

The dynamics of antiphase-boundary motion is investigated by the emerging method of x-ray photon correlation spectroscopy. Time correlations of intensity fluctuations from the fundamental (110) and from the superstructure (100) reflection of the B2-ordered $Co_{60}Ga_{40}$ intermetallic phase are analyzed. By applying detrended fluctuation analysis the observed correlation behavior can be unambiguously attributed to dynamics of antiphase domains. From the temperature dependence an activation energy for this dynamics is derived—in good agreement with results from Monte Carlo simulations. The study underlines the potential of the method for investigations of slow dynamics in hard-condensed matter.

DOI: 10.1103/PhysRevB.69.224301 PACS number(s): 81.05.Bx, 61.10.Eq, 05.40.−a

I. INTRODUCTION

Although the mathematical basic description of crystalline solids suggests perfectly ordered entities, actually they contain a lot of disorder, ranging from zero-dimensional to many-dimensional defects. In the case of ordered alloys current defects are antiphase domains resulting from the growth of a superstructure from different nucleation centers in the alloy. Scattering experiments provide an opportunity to gain information on these antiphase domains. In a classical scattering experiment incoherent x rays are used and therefore only information about average sample properties can be gained. Note that the term "incoherent x rays" solely refers to the modest coherence properties of the used radiation, i.e., very small coherence lengths, and not to a noncollective scattering event. By measuring the width of the superstructure reflection the mean antiphase-domain size can be determined.

The situation changes if coherent radiation is used. The diffraction pattern is then directly related to the positions of all individual scattering centers in the illuminated sample volume. Disorder in the sample, e.g., antiphase domains, causes a highly modulated scattering intensity, called speckle pattern. A decade ago Sutton *et al.* reported the first experiment with partially coherent x rays where such a (static) speckle pattern was resolved in the superstructure peak of Cu_3Au. [1] Now, if the sample undergoes dynamics, i.e., scattering centers change their positions, the corresponding speckle pattern also changes, yielding fluctuating speckle intensities. Analyzing their temporal correlations, which is usually done by calculating (auto) correlation functions, gives information about the underlying dynamics. This is the principle of x-ray photon correlation spectroscopy (XPCS), which was up to now mainly applied to soft-condensed matter problems, e.g., Refs. 2–7 and less in hard-condensed matter physics. [8–11]

In this paper we show that with today's available synchrotron radiation sources it is even possible to study the *dynamics* of antiphase domains, which is synonymous for the movement of antiphase boundaries, using XPCS in combination with an unconventional data evaluation technique. In order to reveal temporal correlations in fluctuating speckle intensities in the superstructure (100) peak and in the fundamental (110) reflection of the intermetallic B2-ordered phase $Co_{60}Ga_{40}$, we apply detrended fluctuation analysis (DFA). Originally, this technique was invented for detecting spatial long-range correlations in nucleotide sequences of DNA [12] and is based on fluctuation analysis (FA), which was used as "DNA walk analysis." [13] Recently, we used FA to study long-term correlations in time series of fluctuating x-ray speckle intensities measured in small angle x-ray spectra of phase-separating alloys.[14] However, the detection of long-term correlations, that correspond to a power-law decay of the autocorrelation function $C(t) \propto t^{-\gamma}$ with $0 < \gamma < 1$ and t the time, is hindered by the presence of smooth trends in the data in addition to random fluctuations. Trends caused by, e.g., a nonconstant overall intensity during the measurement, will conceal the correlation behavior if they are not being taken care of. $C(t)$ always becomes statistically very unreliable for large t, and in the presence of trends it shows artifacts. While the first problem is avoided by FA, we need to subtract the smooth trends from the data ("detrending" of the data) in order to deal with the second problem.[15] Thus, we apply the DFA method, which can also analyze nonstationary data, e.g., random-walk processes, where the autocorrelation function $C(t)$ is not well defined because of a nonconstant mean value of the intensity. In addition, the DFA can reliably distinguish stationary and nonstationary scaling regimes within time series governed by more than one process.

II. EXPERIMENTAL DETAILS AND DATA EVALUATION

A single crystal of the intermetallic B2 phase $Co_{60}Ga_{40}$ was grown using the Bridgman technique. The B2 structure (or CsCl structure) is a body-centered cubic (bcc) crystal structure, where one sort of atom sits in the cube center,

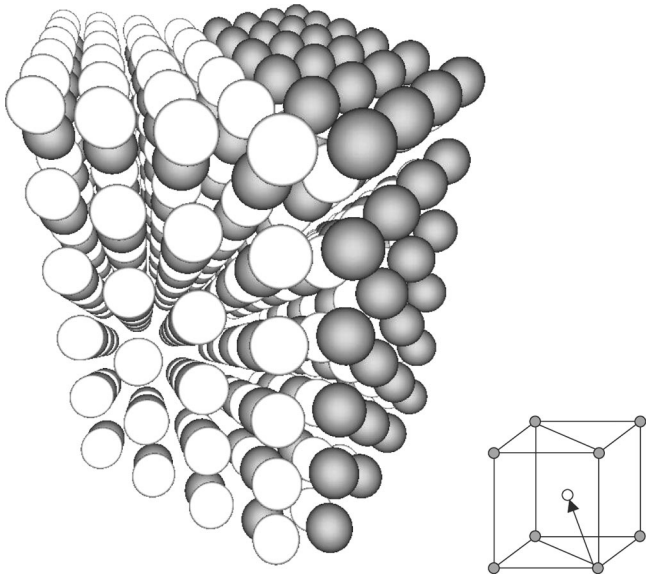

FIG. 1. Schematic illustration of antiphase domains in the B2 structure. The inset shows the B2 structure and the vector in the (110) plane, about which domains are shifted to each other.

whereas atoms of the other sort occupy the cube corners. This superstructure, as compared to the underlying bcc structure, is not homogeneously established over the whole crystal and antiphase domains occur. They are caused by a relative shift in (110) planes by displacement vectors $\langle \frac{1}{2}\frac{1}{2}\frac{1}{2} \rangle$, see Fig. 1. In the case of our sample, disorder is also introduced by a significant fraction of thermally induced vacancies and, predominantly, by a large amount of antistructure Co atoms.[16] These kinds of disorder result in a diffuse scattering intensity into 4π solid angle, thus not disturbing our measurements in Bragg directions.

Two samples with different orientations were cut and polished—with the surface being a (100) lattice plane and a (110) plane, respectively. The idea was to make the same measurements both at the (100) superstructure peak and at the (110) fundamental reflection, in order to check whether dynamics measured at the (100) superstructure peak can exclusively be attributed to fluctuations of antiphase domains. If yes, then no correlations should be seen in data taken at the (110) fundamental reflection, which is caused by the unaffected bcc structure.

Measurements were performed in scattering geometry with a specially constructed furnace with a large capton window covering an angular range of almost 180°. The surface temperature of the sample was calibrated by Mössbauer spectroscopy measuring the second order Doppler shift of a paramagnetic B2-ordered FeAl sample. This means that all given temperature values correspond $\pm 10\,^{\circ}\mathrm{C}$ to the real surface temperature of our sample and not just to the temperature of a thermocouple which was mounted close to the sample surface.

All x-ray measurements were performed at the undulator beamline ID10A at the European Synchrotron Radiation Facility, Grenoble. The x-ray energy of exactly 8 keV was selected by a Si(111) monochromator, corresponding to a wavelength of 1.55 Å. Temporal coherence was achieved by an energy resolution of $\Delta E/E = 10^{-4}$, yielding a longitudinal coherence length $\xi_l \approx \lambda^2/\Delta\lambda \approx 1.5\ \mu$m. This sets the limit for the x-ray path length difference (PLD) up to where interference is possible. In reflection geometry, this is PLD $\approx 2\ \mu \sin^2\Theta$, with μ the attenuation length of the sample ($\mu \approx 5.44\ \mu$m for $Co_{60}Ga_{40}$) and Θ the half scattering angle. The typical transversal coherence length was about 10 μm.[17] The spatial coherence of the beam was therefore ensured by placing a circular pinhole of diameter $d = 8\ \mu$m about 20 cm upstream of the sample.

Pictures ("frames") of the speckle patterns were taken with a charge coupled device (CCD) camera (Princeton Instruments, directly illuminated chip, 1242×1152 pixels, pixel size $22.5 \times 22.5\ \mu\mathrm{m}^2$). When investigating the (100) superstructure peak at a scattering angle $2\Theta \approx 31.2°$ the camera was mounted on a table in $D = 2.3$ m distance from the sample. Due to spatial limitations for the experimental setup at ID10A this distance had to be reduced to $D = 1.71$ m when the (110) Bragg peak at $2\Theta \approx 44.8°$ was measured. Even at this shorter distance the estimated speckle size $(\lambda/d)D \approx 33\ \mu$m was well above the pixel size of the CCD camera, which guaranteed a sufficient resolution of the expected speckle pattern. Also the coherence condition PLD $\lesssim \xi_l$ was fulfilled for both measurements. In order to save readout time rectangular regions of interest that covered a certain area around the peak were read out. The repetition rate was the sum of the times for exposure (0.15–2 s) and for readout (0.48 s for a typical area of 300×300 pixels).

We demonstrate the effect of coherent illumination by means of Fig. 2, which shows the sum of 200 frames of the (100) superstructure peak measured at room temperature. No dynamics is seen and a static speckle pattern with a pronounced and clearly visible structure is obtained. This is further illustrated by a slice across the peak. Strong spatial intensity fluctuations are found due to interferences from all scattering centers in the coherently illuminated volume. If incoherent scattering had been used, an ensemble average from many regions in the illuminated sample would have built up. This is indicated by the dashed line, which is a Gaussian fit to the measured intensity distribution. The mean size of the antiphase domains can be estimated from the width of this curve via the Scherrer formula[18] to 400 ± 15 nm.

For dynamics investigations our samples were measured at temperatures up to 785 °C. Time series of up to $N = 4096$ frames were taken. In order to obtain information about temporal correlations, the intensity-time series of pixels lying in a circular region around the peak center shown in Fig. 2 were analyzed by first, second, and third order DFA.[12,15] For this we consider, for each pixel, the integrated time series ("profile")

$$Y(j) = \sum_{k=1}^{j} \Delta I_k \tag{1}$$

of the intensity fluctuations $\Delta I_k = I_k - \langle I \rangle$, with I_k the intensity in the kth time bin and $\langle I \rangle = (1/N)\Sigma_{k=1}^{N} I_k$ the mean intensity in the considered pixel. We divide the profile $Y(j)$ into nonoverlapping segments of size t. Here, t will be the scaling

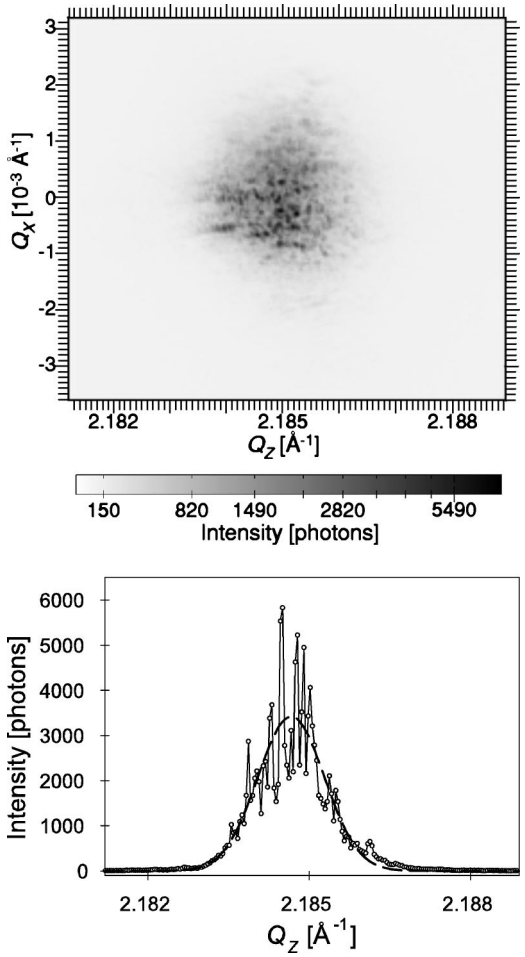

FIG. 2. Illustration of the effect of coherent scattering. Top: sum of 200 CCD images of the (100) superstructure peak at room temperature, logarithmic intensity scale, Q_z normal to the sample plane, Q_x normal to the scattering plane. Bottom: slice through the peak exhibiting strong intensity fluctuations, $Q_x=0$ Å^{-1}, linear intensity scale. The dashed line indicates a Gaussian fit to the intensity distribution—this would be the result of scattering with conventional, incoherent x rays.

variable, i.e., the aim is to measure the fluctuations on the time scale t while simultaneously eliminating trends (detrending of the data). For DFA of order n (DFAn), in each segment $Y(j+1)$ to $Y(j+t)$ (or equivalently $Y(j+i)$ with $i=1,\ldots,t$), the best fit of a polynomial $p_j(i)$ of order n is determined. In this way, trends of order n in the profile and of order $n-1$ in the raw data, respectively, are removed. Then the variance of the profile $Y(j+i)$ from the polynomial $p_j(i)$ is calculated

$$F_j^2(t) = \frac{1}{t}\sum_{i=1}^{t} [Y(j+i) - p_j(i)]^2. \qquad (2)$$

Finally, we average $F_j^2(t)$ over all segments and over all pixels under consideration to improve statistics and obtain the average square of the so-called fluctuation function. At last the square root is taken to get $F(t)$.

Here, we are mainly interested in distinguishing two types of fluctuation-scaling behavior, uncorrelated behavior and diffusion (random walk) behavior. If the intensity fluctuations ΔI_k are uncorrelated, the scaling behavior of the profile $Y(j)$ [Eq. (1)] can be understood in analogy to the random walk of a particle in one dimension in space. Calculating $Y(j)$ would give the particle position after j time steps if ΔI_k denoted the *step* of the particle at time step k. The square of the DFA fluctuation function $F^2(t)$ would correspond to the (detrended) mean-square displacement of the particle after t time steps. Assuming random uncorrelated motion, $F^2(t)$ would be given by the well-known Einstein relation $F^2(t)=2Dt=2Dt^{2\alpha}$ with $\alpha=1/2$ and D the diffusivity. Hence, we expect $\alpha=1/2$ for uncorrelated intensity fluctuations.

If, on the other hand, the intensity fluctuations ΔI_k are given by a random walk, i.e., if they correspond to the *position* of a diffusing particle, the mean of ΔI_k itself already increases as $\langle \Delta I_k \rangle \propto k^{1/2}$. Of course, such nonstationary behavior cannot occur for all time scales, since the mean $\langle I \rangle$ would not be defined. But such behavior can occur for intermediate time scales. In this case the calculation of the profile $Y(j)$ [Eq. (1)] involves an additional summation over time (or integration if considered as a continuous process). This integration increases the scaling exponent α by one, leading to $F(t) \propto t^{\alpha}$ with $\alpha=3/2$ for the scaling behavior of the DFA fluctuation function in the considered intermediate scaling regime.

Note that such behavior cannot be detected when the standard FA is considered, since the scaling exponent is constrained by $\alpha<1$ in that case. Neither can the autocorrelation function reveal such scaling behavior, since stationarity of the series is assumed for all time scales in that approach. However, the DFA can handle this situation. In addition, trends in the data might look like random-walk behavior and thus lead to spurious results with $\alpha>1$. Successively applying DFA of higher order removes these trends, i.e., only the real scaling behavior remains.

Intermediate values of α can be interpreted as follows: If $F(t)$ increases as t^{α} with $1/2<\alpha<1$, the data is power-law long-term correlated corresponding to an autocorrelation function $C(t) \propto t^{-\gamma}$ with $\gamma=2-2\alpha$. If $\alpha=1$, the data show $1/f$ noise scaling, [19] which is just on the edge of nonstationarity. If $1<\alpha<3/2$, the data correspond to a random walk with anticorrelated steps, which is less nonstationary than a random walk with uncorrelated steps.

III. RESULTS AND DISCUSSION

Figure 3 shows fluctuation functions $F(t)$ from DFA1, DFA2 and DFA3 evaluations (from top to bottom) at different temperatures for the (100) superstructure peak (left-hand side) and the (110) fundamental reflection (right-hand side). The first obvious feature is that in all plots for the (100) superstructure peak the intensity fluctuations at room temperature do not show any signs of diffusion behavior, which manifests as a straight line with slope $\alpha=0.5$ (gray dashed lines as eye guidance) in the double-logarithmic diagram. This means that at room temperature no dynamics takes

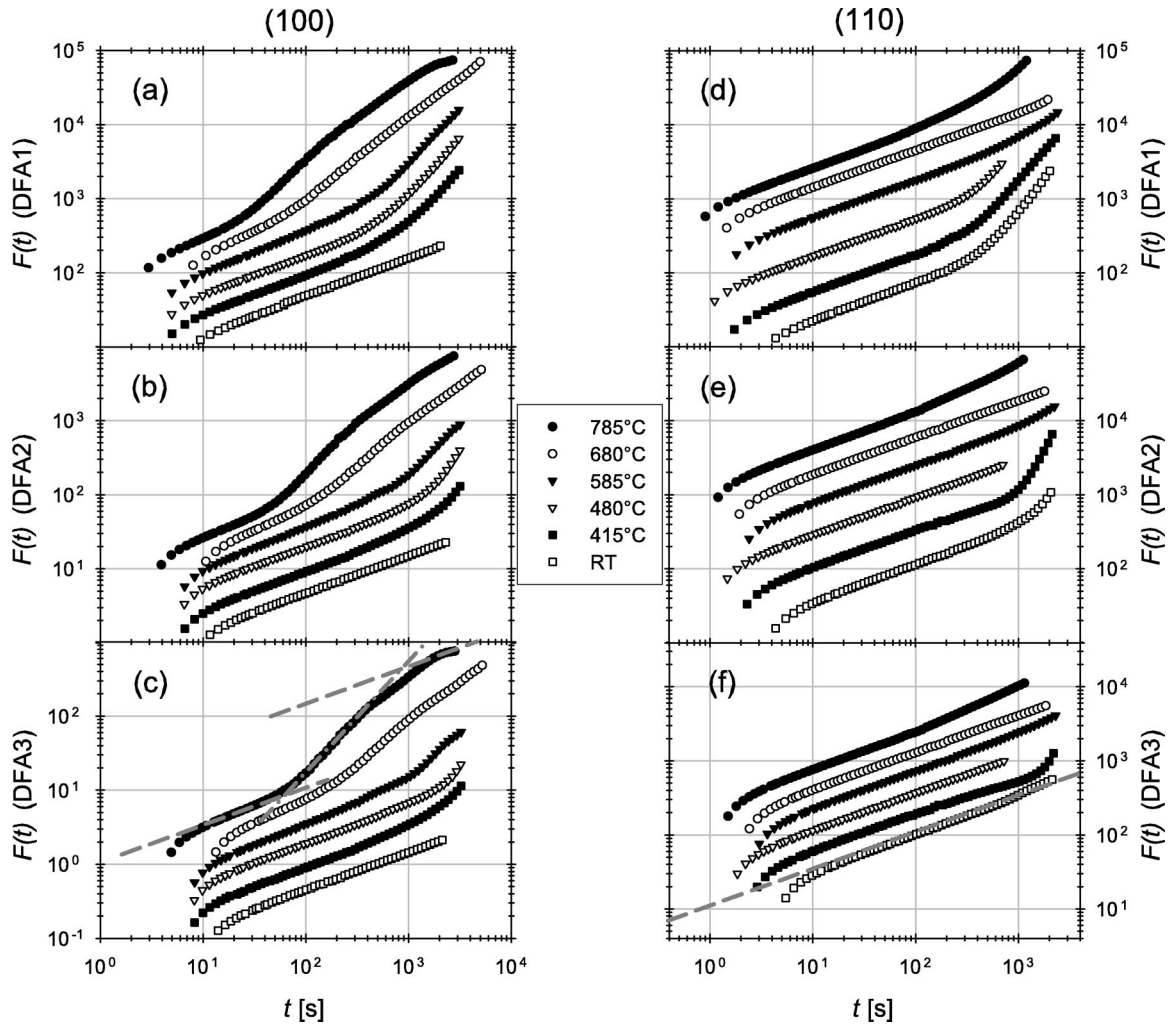

FIG. 3. From top to bottom: results from data analysis with DFA1 (a, d), DFA2 (b, e) and DFA3 (c, f). Curves are shifted along the *y* axis for clarity. Left: (100) superstructure peak (a, b, c). Right: (110) fundamental reflection (d, e, f). Notice the effect of detrending with higher order DFA. In the fluctuation functions $F(t)$ of the fundamental reflection no indications for random-walk fluctuations ($\alpha=1.5$) are visible after applying third order DFA (f), in contrast to fluctuation functions of the superstructure peak (c). Dashed lines indicate slope 0.5 and the dash-dotted line slope 1.5, respectively.

place within the total duration of the measurements, which is of course the reason why the pronounced speckle structure is preserved in the summation of 200 CCD frames, shown in Fig. 2.

The next eye-catching detail is that the set of fluctuation functions $F(t)$ for different temperatures is qualitatively the same for all three orders of DFA in case of the superstructure peak. There, for all temperatures greater than room temperature a crossover is observed from slope $\alpha=0.5$ to $\alpha=1.5$ (gray dash-dotted line as eye guidance). This means, intensity fluctuations that make a random walk ("random-walk fluctuations") are observed on longer time scales in contrast to uncorrelated random noise on short time scales. Furthermore, the crossovers occur at shorter times the higher the temperature was, i.e., the ratio of the amplitudes of random-walk fluctuations to uncorrelated fluctuations is shifted to random-walk fluctuations with higher temperatures. Thus, the underlying process must be thermally activated, like dynamics of antiphase domains. Looking more carefully one recognizes a shift of all crossovers to longer time scales with increasing order of detrending. This behavior as well as the curvature of the first few points in each fluctuation function $F(t)$ is simply an attribute of the DFA method. For a more detailed description we refer to Ref. 15 , where a technique for the determination of the real crossover time can also be found, although the absolute time is not important in our case. Additionally, at the three highest temperatures (585 °C, 680 °C, and 785 °C) another, slower crossover to slope $\alpha=0.5$, asymptotically, is visible on long time scales, which is best seen in the DFA3 plot, Fig. 3(c).

What is the reason for this slow crossover to $\alpha=0.5$ again, after $\alpha=1.5$ indicating a random walk of speckle intensities? Although we measure intensities it is phase information that is retrieved, because the phasing of the scattered photons determines the detected intensity fluctuations. On principle, any phase information is modulo 2π. After an additional

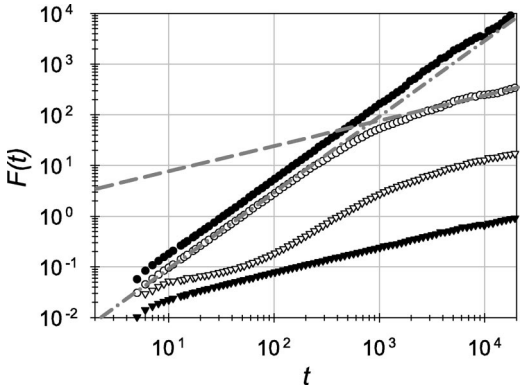

FIG. 4. Illustration of DFA3 results for a random walk of phases by means of simulated data. DFA3 was computed for random numbers, full triangles, for a one-dimensional random walk due to these random numbers, full circles, for $\sin^2$ of this random walk, open circles, and for $\sin^2$ of the random walk with a random uncorrelated background present, open triangles. Curves are shifted along the y axis for clarity. The dashed line indicates $\alpha=0.5$ and the dash-dotted line $\alpha=1.5$, respectively.

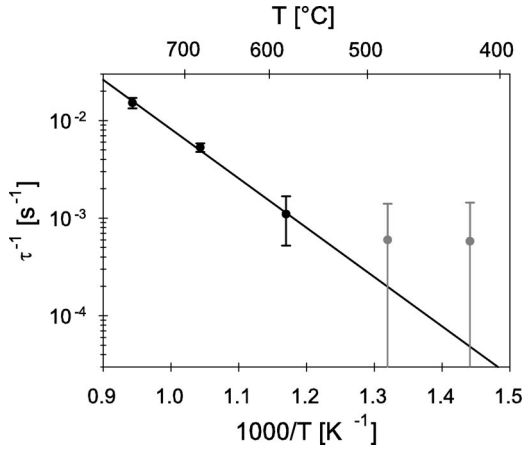

FIG. 5. Results for the crossover time τ from fits of DFA3 spectra, plotted in an Arrhenius diagram. Due to the small number of points after the crossover at 415 °C and 480 °C, see Fig. 3(c), fits of these two spectra are not very significant and crossover times are plotted in gray. Hence, only the results for the three highest temperatures were taken for determining an activation energy by fitting $\propto\exp(-E_{\mathrm{APB}}/k_BT)$, straight line, yielding $E_{\mathrm{APB}}=1.05\pm0.10$ eV.

phase difference of 2π between interfering scattered waves is exceeded the situation becomes indistinguishable from the initial state. Hence, $\alpha>0.5$ is not possible on very large time scales provided the underlying dynamics is sufficiently fast. Figure 4 illustrates the situation by means of simulated data. Diagrammed are DFA3 analyses of random numbers, full triangles, of a one-dimensional random walk due to these random numbers, full circles, of the square sine of this random walk, open circles, and of the square sine of the random walk together with a background of random uncorrelated numbers, open triangles. The sine of the random walk represents a random walk of phases, which is also present in the amplitudes of the scattered photons due to the diffusion dynamics in our sample. In the experiment we measure intensities, i.e., the modulus squared of amplitudes. Thus, the DFA3 result for $\sin^2$ (and not just for the sine) of the simulated random walk is plotted in Fig. 4, open circles. In order to maximize the analogy to the measurement we added a random uncorrelated background to $\sin^2$ of the simulated random walk and also plotted the DFA3 result for this signal, Fig. 4, open triangles. One can easily recognize the characteristic behavior of the fluctuation functions $F(t)$: $\alpha=0.5$ on all time scales for uncorrelated random numbers, $\alpha=1.5$ on all time scales for a random walk and a slow crossover from $\alpha=1.5$ (indicated by the gray dash-dotted line) to $\alpha=0.5$ (indicated by the gray dashed line) on long time scales for the square of a random walk of phases. Finally, we find $\alpha=0.5$ also on short time scales for the square of a random walk of phases when a random uncorrelated background is present.

The DFA results for the (110) fundamental peak are in contrast to all these observations, Figs. 3(d)–3(f). There, a dramatic effect of detrending is visible. After applying third order DFA all fluctuation functions exhibit approximately $\alpha=0.5$ on all time scales. Therefore, all crossovers from $\alpha=0.5$ to $\alpha>0.5$ in the DFA1 and DFA2 spectra are due to trends and do not mirror real correlations, which corroborates the necessity for applying a detrending technique. This means that we do not see any correlations and no signs of diffusive behavior in the data of the fundamental reflection, which makes it possible to attribute the random-walk fluctuations seen in the superstructure-peak data to dynamics of antiphase domains, exclusively.

As stated above the shift of the crossover from $\alpha=0.5$ to $\alpha=1.5$ in the DFA spectra of the (100) peak indicates a temperature-activated process, proportional to $\exp(-E_{\mathrm{APB}}/k_BT)$, with E_{APB} the activation energy and k_B Boltzmann's constant. In order to determine E_{APB} we fixed the crossover times τ (by the interception of straights that were fitted in the regions of constant slope before and after the crossover) as a function of the temperature and graphed them in an Arrhenius plot, Fig. 5. This was done using the DFA3 spectra since they are least affected by trends. Because only a few data points remain after the crossover in the case of the DFA3 curves at 415 and 480 °C the determined crossover times are not very significant for these two temperatures. Therefore, just the three points for 585, 680, and 785 °C in the Arrhenius plot were fitted $\propto\exp(-E_{\mathrm{APB}}/k_BT)$ in order to determine the activation energy E_{APB}. This fit, represented by the straight line in Fig. 5, gives an activation energy for the motion of antiphase boundaries of $E_{\mathrm{APB}}=1.05\pm0.10$ eV.

The above determination of the activation energy is based on the assumption that the uncorrelated random noise, which is mainly caused by the nonperfect coherence of the beam and which is responsible for $\alpha=0.5$ on short time scales, does not significantly change from measurement to measurement. Otherwise it could be imaginable that, by incident, the amplitude of the uncorrelated random noise decreased from the measurements at low temperatures to the measurements at high temperatures, thus causing the crossovers from $\alpha=0.5$ to $\alpha=1.5$ to appear at shorter and shorter times τ. This

scenario can be excluded, however, by looking at the crossovers from $\alpha=1.5$ to $\alpha=0.5$, at the three highest temperatures, Fig. 3(c). As explained above, this crossover is caused by the fact that, effectively, a random walk of the phases of the scattered photons is detected, corresponding to the dynamics in the sample. The time at which this crossover occurs is solely determined by how fast the dynamics in the sample takes place, i.e., this crossover time should be the same at all temperatures if only the amplitude of the uncorrelated random noise differed from measurement to measurement. Figure 3(c) demonstrates that the latter does not apply to our case, because the crossover from $\alpha=1.5$ to $\alpha=0.5$ (visible for 585, 680, and 785° C) shifts to shorter times with higher temperatures, indicating thermally activated dynamics in the sample as reason. Additionally, we checked these three crossover times and found the same ratios between them as between the times for the first crossover from $\alpha=0.5$ to $\alpha=1.5$. Hence, the above determination of the activation energy E_{APB} is justified.

For a better understanding of the result $E_{\mathrm{APB}}=1.05\pm0.10$ eV we consider data from Monte Carlo simulations of atomic diffusion via a vacancy mechanism in a B2-ordered model alloy, where the mobility M of antiphase boundaries was also examined.[20] Coarsening of antiphase domains was confirmed to follow a power law, $R(t)\propto(Mt)^{1/2}$ (Allen–Cahn law), [21] with R the mean domain size. A quantitative analysis yielded an activation energy of the antiphase-domain mobility about a factor 3.5–4.2 smaller than the activation energy for the diffusion process (for details we refer to Ref. 20). We note that since the number of vacancies is fixed to 1 in the Monte Carlo simulation [20] the derived activation energies are only migration energies—without a formation-energy term. The rather small energies for the antiphase-domain mobility can be understood in comparison with Monte Carlo simulations that indicated that the vacancy path is mainly restricted to disordered regions, [22] i.e., to antiphase boundaries. This means that we can compare our result with data from diffusion experiments on $Co_{60}Ga_{40}$.

Fortunately, there exist detailed tracer diffusion studies in the CoGa system. [23] For our sample composition and the relatively low temperatures diffusion of Co atoms can be described by nearest-neighbor jumps between regular Co sites and anti-structure sites via single vacancies. Furthermore, quasielastic neutron scattering studies[24] showed that this is the elementary jump of Co in CoGa. We add that for higher temperatures Stolwijk, van Gend, and Bakker, [23] proposed a so-called triple-defect mechanism for the Co diffusion to account for the upward curvature of the tracer diffusion coefficient and the coupling of Co and Ga diffusion. But Monte Carlo simulations showed that a more general diffusion mechanism based on nearest-neighbor jumps is also able to explain the experimental findings.[25,26]

The tracer diffusion measurements yield an activation energy for the Co diffusion in $Co_{60}Ga_{40}$ of $E_D=2.24\pm0.07$ eV. [23] Since the diffusivity of Co atoms is much higher than the diffusivity of Ga atoms (about a factor of 15 at 700 °C, increasing with decreasing temperature) we can disregard Ga diffusion completely. As stated above, the Monte Carlo simulation dwells on the vacancy-migration energy. Consequently, we need to subtract the value for the vacancy-formation energy, E_D^f, from the activation energies found in the tracer diffusion measurements (E_D) and our XPCS experiment (E_{APB}). Regrettably, we have no exact information about E_D^f in $Co_{60}Ga_{40}$. But, from the work of van Ommen and Miranda [16] we can estimate this value, at least. This, because in Ref. 16 values for the vacancy-formation energy for five compositions between $Co_{48}Ga_{52}$ (0.15 eV) and $Co_{56}Ga_{44}$ (0.50 eV) are given. Extrapolation yields $E_D^f=0.66\pm0.15$ eV for our sample composition. Subtracting this value we end up with $E_D^m\equiv E_D-E_D^f=1.58\pm0.17$ eV, $E_{\mathrm{APB}}^m\equiv E_{\mathrm{APB}}-E_D^f=0.39\pm0.18$ eV, and $E_D^m/E_{\mathrm{APB}}^m=4.1\pm1.9$, respectively, in good agreement with the Monte Carlo simulation results.[20] Table I presents a compilation of these findings.

TABLE I. Compilation of the results from simulations and measurements. Presented are the activation energy for atomic diffusion E_D, the vacancy formation energy E_D^f, the vacancy migration energy E_D^m, the activation energy for the motion of antiphase boundaries E_{APB}, the migration energy for the motion of antiphase boundaries E_{APB}^m, and the ratio between E_D^m and E_{APB}^m.

	Simulation	Measurements
E_D	⋯	2.24±0.07 eV[b]
E_D^f	⋯	0.66±0.15 eV[c]
E_D^m	23.0–24.1J$^{(1)}$[a]	1.58±0.17 eV
E_{APB}	⋯	1.05±0.10 eV
E_{APB}^m	5.5–6.8J$^{(1)}$[a]	0.39±0.18 eV
E_D^m/E_{APB}^m	3.5–4.2	4.1±1.9

[a]From Ref. 20, where the unit of energy, $J^{(1)}$, is defined via ordering energies $J^{(k)}$ between kth nearest-neighbor atoms.
[b]From Ref. 23.
[c]Extrapolated from values given in Ref. 16.

In conclusion, we successfully applied detrended fluctuation analysis to data of an x-ray photon correlation spectroscopy experiment. Thereby, we followed the dynamics in the superstructure peak of a $Co_{60}Ga_{40}$ B2-ordered single crystal. By comparison with data taken at the fundamental reflection we attribute the measured dynamics to motion of antiphase-domain boundaries. Furthermore, the activation energy E_{APB} for the mobility of the antiphase boundaries was determined. As predicted by Monte Carlo simulations subtracting the vacancy-formation energy E_D^f from E_{APB} gives approximately a quarter of the migration energy for diffusion of Co atoms. The presented study underlines the potential of the method for investigations of slow dynamics in hard-condensed matter, particularly when it is necessary to account for spurious correlations and trends, respectively.

ACKNOWLEDGMENTS

This work was financially supported by the Austrian Federal Ministry for Education, Science and Culture (Project No. GZ 45.529/2-VI/B/7a/2002) and the Hahn-Meitner-Institut Berlin in cooperation with the University of Potsdam. Data were evaluated using the Schrödinger II cluster of the Vienna University Computer Center.

*Electronic address: lstadler@ap.univie.ac.at
†Present address: Deutsches Elektronen Synchrotron (Hasylab), Notkestraße 85, D-22607 Hamburg, Germany.

[1] M. Sutton, E. E. Nagler, S. G. Mochrie, T. Greytak, L. E. Bermann, G. Held, and G. B. Stephenson, Nature (London) **352**, 608 (1991).
[2] T. Thurn-Albrecht, W. Steffen, A. Patkowski, G. Meier, E. W. Fischer, G. Grübel, and D. L. Abernathy, Phys. Rev. Lett. **77**, 5437 (1996).
[3] S. G. J. Mochrie, A. M. Mayes, A. R. Sandy, M. Sutton, S. Brauer, G. B. Stephenson, D. L. Abernathy, and G. Grübel, Phys. Rev. Lett. **78**, 1275 (1997).
[4] D. O. Riese, W. L. Vos, G. H. Wegdam, F. J. Poelwijk, D. L. Abernathy, and G. Grübel, Phys. Rev. E **61**, 1676 (2000).
[5] D. Lumma, M. A. Borthwick, P. Falus, L. B. Lurio, and S. G. J. Mochrie, Phys. Rev. Lett. **86**, 2042 (2001).
[6] A. Madsen, J. Als-Nielsen, and G. Grübel, Phys. Rev. Lett. **90**, 085701 (2003).
[7] T. Thurn-Albrecht, F. Zontone, G. Grübel, W. Steffen, P. Müller-Buschbaum, and A. Patkowski, Phys. Rev. E **68**, 031407 (2003).
[8] S. Brauer, G. B. Stephenson, M. Sutton, R. Brüning, E. Dufresne, S. G. J. Mochrie, G. Grübel, J. Als-Nielsen, and D. L. Abernathy, Phys. Rev. Lett. **74**, 2010 (1995).
[9] A. Malik, A. R. Sandy, L. B. Lurio, G. B. Stephenson, S. G. J. Mochrie, I. McNulty, and M. Sutton, Phys. Rev. Lett. **81**, 5832 (1998).
[10] F. Livet, F. Bley, R. Caudron, E. Geissler, D. Abernathy, C. Detlefs, G. Grübel, and M. Sutton, Phys. Rev. E **63**, 036108 (2001).
[11] S. Francoual, F. Livet, M. de Boissieu, F. Yakhou, F. Bley, A. Létoublon, R. Caudron, and J. Gastaldi, Phys. Rev. Lett. **91**, 225501 (2003).
[12] C.-K. Peng, S. V. Buldyrev, S. Havlin, M. Simons, H. E. Stanley, and A. L. Goldberger, Phys. Rev. E **49**, 1685 (1994).
[13] C.-K. Peng, S. V. Buldyrev, A. L. Goldberger, S. Havlin, F. Sciortino, M. Simons, and H. E. Stanley, Nature (London) **356**, 168 (1992).
[14] L.-M. Stadler, B. Sepiol, R. Weinkamer, M. Hartmann, P. Fratzl, J. W. Kantelhardt, F. Zontone, G. Grübel, and G. Vogl, Phys. Rev. B **68**, 180101(R) (2003).
[15] J. W. Kantelhardt, E. Koscielny-Bunde, H. H. A. Rego, S. Havlin, and A. Bunde, Physica A **295**, 441 (2001).
[16] A. H. van Ommen and J. de Miranda, Philos. Mag. A **43**, 387 (1981).
[17] C. Gutt, T. Ghaderi, V. Chamard, A. Madsen, T. Seydel, M. Tolan, M. Sprung, G. Grübel, and S. K. Sinha, Phys. Rev. Lett. **91**, 076104 (2003).
[18] B. D. Cullity, *Elements of X-ray Diffraction*, 2nd ed. (Addison–Wesley, Read MA, 1978).
[19] D. Sornette, *Critical Phenomena in Natural Sciences* (Springer, Berlin, 2000)
[20] R. Weinkamer, P. Fratzl, B. Sepiol, and G. Vogl, Phys. Rev. B **58**, 3082 (1998).
[21] S. M. Allen and J. W. Cahn, Acta Metall. **27**, 1085 (1979).
[22] E. Vives and A. Planes, Int. J. Mod. Phys. C **4**, 701 (1993).
[23] N. A. Stolwijk, M. van Gend, and H. Bakker, Philos. Mag. A **42**, 783 (1980).
[24] M. Kaisermayr, J. Combet, H. Ipser, H. Schicketanz, B. Sepiol, and G. Vogl, Phys. Rev. B **63**, 054303 (2001).
[25] M. Athènes, P. Bellon, and G. Martin, Philos. Mag. A **76**, 565 (1997).
[26] I. V. Belova and G. E. Murch, Philos. Mag. A **81**, 95 (2001).